Broadband Microwave Filters Based on Open Split Ring Resonators (OSRRs) and Open Complementary Split Ring Resonators (OCSRRs): Improved Models and Design Optimization

Miguel DURÁN-SINDREU [1], *Paris VÉLEZ* [1], *Jordi BONACHE* [1], *Ferran MARTÍN* [1]

[1] GEMMA/CIMITEC Departament d'Enginyeria Electrònica, Universitat Autònoma de Barcelona, 08193 BELLATERRA (Barcelona), Spain

Ferran.Martin@uab.es

Abstract. *The paper is focused on the design of broadband bandpass filters at microwave frequencies. The proposed filters are based on a combination of open split ring resonators (OSRRs) and open complementary split ring resonators (OCSRRs) loaded in a host transmission line. Since these resonators (OSRRs and OCSRRs) are electrically small, the resulting filters are compact. As compared to previous papers by the authors on this topic, the main aim and originality of the present paper is to demonstrate that by including a new series inductance in the circuit model of the OCSRR, it is possible to improve the predictions of these filter models and better fit the measured filter responses. Moreover, the parameter extraction method of the new circuit model and an automated filter design technique is introduced and demonstrated. The paper is complemented with the design and comparison of several prototypes.*

Keywords

Bandpass filters, metamaterials, open split ring resonator, open complementary split ring resonator.

1. Introduction

The wideband bandpass filters of the present paper are based on the open versions of the split ring resonator (SRR) [1] and the complementary split ring resonator (CSRR) [2]. SRRs and CSRRs, among other particles [3], [4], have been used for the synthesis of negative effective permeability and permittivity media, respectively, and also for the synthesis of left handed metamaterials. In planar technology, these particles have been used for the implementation of composite right/left handed (CRLH) transmission lines, namely, lines exhibiting backward wave propagation at low frequencies, and forward wave propagation at high frequencies [5], [6], and also for the implementation of broadband filters based on them [7].

However, by using the open versions of the SRR and the CSRR combined, i.e., the open split ring resonator (OSRR) [8] and the open complementary split ring resonator (OCSRR) [9], it has been recently demonstrated the possibility of implementing CRLH lines in both microstrip and coplanar waveguide technology [10] without the presence of a transmission zero below the first (left handed) transmission band (such transmission zero is present in the CRLH lines implemented by using SRRs or CSRRs [5], [6]). It has been also pointed out that by sacrificing periodicity in OSRR- and OCSRR-based CRLH lines, it is possible to implement compact wideband bandpass filters subject to specifications, and several prototype devices covering different orders and bandwidths have been reported [11], [12].

In the present paper we report an improvement of the circuit model of these OSRR and OCSRR-based filters and also a method to automatically synthesize the required filter responses. This new circuit model is necessary to better predict the response of the filter in the upper region of the band-pass and also the upper transition band. The paper is organized as follows: in section 2, the filter topology and the improved circuit model is presented. In section 3, the parameter extraction method to infer the circuit values of the new proposed model is shown. The automated synthesis method is reported in section 4. In section 5, the design of several prototype devices is reported. Finally, the main conclusions are highlighted in section 6.

2. Filter Topology and Circuit Models

The proposed filters are based on alternating sections of host lines loaded with series connected OSRRs and shunt connected OCSRRs. Fig. 1 presents the topology and the formerly proposed lumped element equivalent circuit models of these filter sections, corresponding to CPW technology [10]. CPW is the technology used for the implementation of the OSRR and OCSRR based filters since the circuit model of a microstrip line section loaded with an OSRR is more complex and this complicates the design, as reported in [10].

Essentially, the OSRR and the OCSRR are described by means of series and parallel resonators, respectively. However, some phase shift at resonance occurs, due to the presence of the host line, and the accurate models of the particles must include these parasitic effects (by means of the indicated phase shifting lines). In the OCSRR section, it is necessary to electrically connect the different ground plane regions (by means of backside strips and vias) to avoid the presence of the slot mode. Notice that the circuit models can be simplified, as Fig. 1 illustrates (i.e., $C'_p = 2(C + C_p)$ and $L'_s = 2L + L_s$). The representation of S_{11} in a Smith Chart (Fig. 2) for both structures reveals the need to include the additional elements to account for the phase shift. The dimensions of the OCSRR are: external radius $r_{ext} = 1.6$ mm, width c and distance between the slot rings d are $c = d = 0.2$ mm. The values of the equivalent circuit elements are: $L = 0.65$ nH, $L'_p = L_p/2 = 0.97$ nH, $C'_p = 2(C_p + C) = 3.11$ pF. The dimensions of the OSRR are: $r_{ext} = 1.8$ mm, $c = 0.2$ mm, $d = 0.3$ mm. The values of the equivalent circuit elements are: $C = 0.2$ pF, $L'_s = L_s + 2L = 6.33$ nH, $C_s = 0.511$ pF. The previous element values have been obtained by means of the parameter extraction procedure detailed in [10].

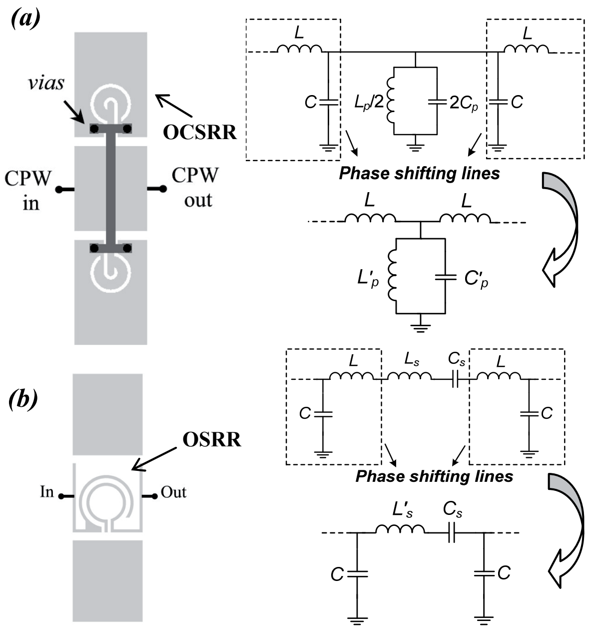

Fig. 1. Topology and circuit model of the OCSRR (a) and OSRR (b) loaded CPW.

The comparison of the insertion and return losses for both structures is depicted in Fig. 3. For the OSRR-loaded CPW section, the agreement between the electromagnetic and circuit simulation is excellent within the frequency range shown. For the OCSRR structure, it can be appreciated that some discrepancy appears at high frequencies. This is due to the connection between the central strip of the CPW transmission line and the inner metallic region of the OCSRR, which generates an inductive effect in series with the shunt resonator. Hence, in order to consider this particle for applications where a prediction far below and beyond the resonance frequency is required, such as wideband devices, this additional inductive effect should be taken into account. Fig. 4 shows the resulting wideband circuit model of an OCSRR-loaded CPW transmission line, where the approach of considering that the shunt capacitances C could still be absorbed by C'_p regardless of the presence of L_{sh} has been considered. The comparison between the electromagnetic and circuit simulation of the wideband response of the structure of Fig. 1(a) is also depicted in Fig. 4, where the parameter extraction method that will be explained in section 3 has been considered to infer the circuit values. It can be appreciated the excellent agreement between both responses when the inductance L_{sh} is included in the model. Indeed, this inductance is responsible for the presence of a transmission zero above the pass-band of the structure, and it is of interest to improve the filter selectivity at the upper transition band.

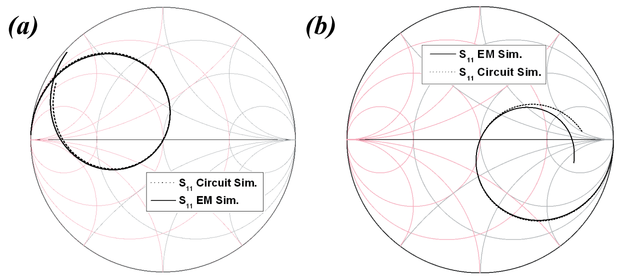

Fig. 2. Representation of S_{11} for the OCSRR (a) and OSRR (b) structures of Fig. 1, implemented on the *Rogers RO3010* substrate with thickness $h = 0.254$ mm and dielectric constant $\varepsilon_r = 11.2$;

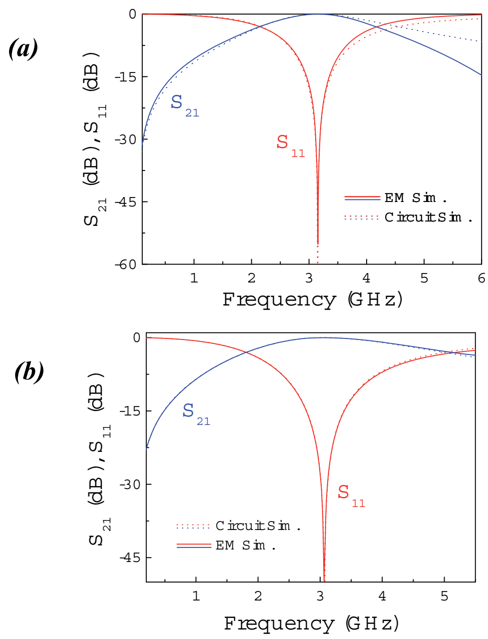

Fig. 3. Insertion and return losses for the structures of Fig. 1. (a) OCSRR-loaded CPW section; (b) OSRR-loaded CPW section.

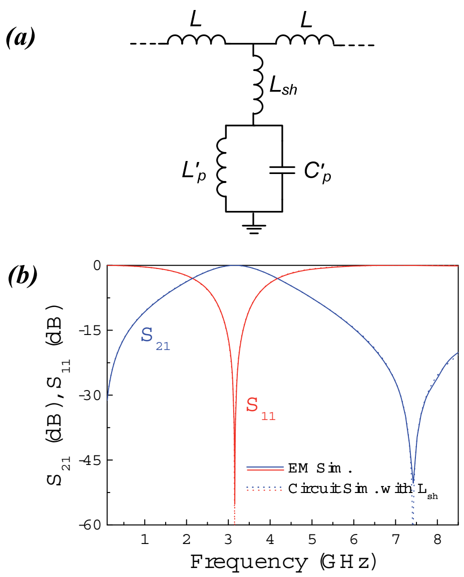

Fig. 4. Wideband circuit model (a) and frequency response (magnitude) (b) of the pair of shunt connected OCSRRs shown in Fig. 1(a). The element values inferred by the parameter extraction method are: $L = 0.345$ pF, $L'_p = 0.94$ nH, $C'_p = 2.98$ pF and $L_{sh} = 0.185$ nH.

3. Parameter Extraction Method of the OCSRR Wideband Circuit Model

The parameters of the circuit model of Fig. 4 can be inferred from the electromagnetic simulation through close equations following a similar methodology as the one explained in [10]. The series inductance can be obtained from the intercept of the return losses with the unit resistance circle in the Smith chart, yielding

$$L = \frac{\chi}{2\omega|_{Z_p\to\infty}} \tag{1}$$

where χ is the reactance at the intercept point. Additionally, the LC tank resonates at this frequency, that is

$$\omega^2|_{Z_p\to\infty} = \frac{1}{L'_p C'_p}. \tag{2}$$

Another condition can be obtained from the reflection zero frequency ω_z, where the characteristic impedance Z_0 is 50 Ω and is given by

$$Z_0(\omega) = \sqrt{Z_s(\omega)[Z_s(\omega) + 2Z_p(\omega)]} \tag{3}$$

where Z_s and Z_p are the series and shunt impedance of the T-circuit model of Fig. 4(a), respectively. Finally, the last condition is obtained from the point at which the electrical length βl is 90º, given by

$$\cos\beta l = 1 + \frac{Z_s(\omega)}{Z_p(\omega)}. \tag{4}$$

Therefore, from equations (2)-(4), all the parameters of the shunt branch can be obtained as

$$L'_p = \frac{\left(\omega^2|_{Z_p\to\infty} - \omega^2|_{\beta l=90^\circ}\right)\left(\omega_z^2 - \omega^2|_{Z_p\to\infty}\right)\left(\omega_z^2 L^2 - Z_0^2\right)}{2L\omega^2|_{Z_p\to\infty}\,\omega_z^2\left(\omega_z^2 - \omega^2|_{\beta l=90^\circ}\right)}, \tag{5}$$

$$C'_p = \frac{1}{\omega^2|_{Z_p\to\infty} L'_p}, \tag{6}$$

$$L_{sh} = \frac{\dfrac{L\omega^2|_{\beta l=90^\circ}}{\omega^2|_{Z_p\to\infty}} - L'_p - L}{1 - \dfrac{\omega^2|_{\beta l=90^\circ}}{\omega^2|_{Z_p\to\infty}}} \tag{7}$$

being thus all the values univocally determined.

4. Filter Design: An Automatic Optimization Routine

The first step for the design of filters based on OSRRs and OCSRRs is to determine the element values of the canonical circuit model, which is the model that results by cascading the simplified circuits of Fig. 1 without the presence of the parasitics, namely L and C. Normally, the element values of the canonical bandpass filter are inferred from response and frequency transformations from the low pass filter prototype corresponding to a given standard response (Butterworth, Chebyshev, etc.), but this requirement is not actually necessary (indeed, in the examples reported later we have considered Chebyshev responses because of the higher frequency selectivity for a given order).

The second step consists to infer the layout of each section so that the elements of the resonator (obtained from the extraction procedure detailed in [10] and in section 3 for the models of Fig. 1 and Fig. 4, respectively) are those of the canonical circuit model. From the parameter extraction method, we obtain the values of the elements modeling the parasitics. Then we use the accurate model of the different sections (with the parasitic values inferred) and we tailor the resonator values until the specifications are satisfied at the circuit level (bandwidth and selectivity).

Finally, we modify the layout of the resonator until the response coincides with that of the circuit simulation. Following this procedure, the final filter layout can be obtained. Of course, due to the presence of the parasitics, a purely standard response cannot be obtained, but the effects of the parasitics are small and the proposed filter topology is roughly described by the canonical model [10].

The technique used to design this kind of filters has been proven to be simple for small order filters and/or small parasitic elements, since the element tuning to infer the optimum response considering parasitics is realized at the circuit level. Fig. 5 reports an illustrative example corresponding to a 3rd order filter with central frequency $f_0 = 2.9$ GHz, 0.02 dB ripple and 35% fractional bandwidth. This filter has been fabricated on the *Rogers RO3010* substrate with thickness $h = 0.254$ mm and measured dielectric constant $\varepsilon_r = 11.2$, where it has been found that by using thinner substrates the stop-band response is improved (i.e., the first spurious band due to the distributed resonances of the resonators is shifted to higher frequencies).

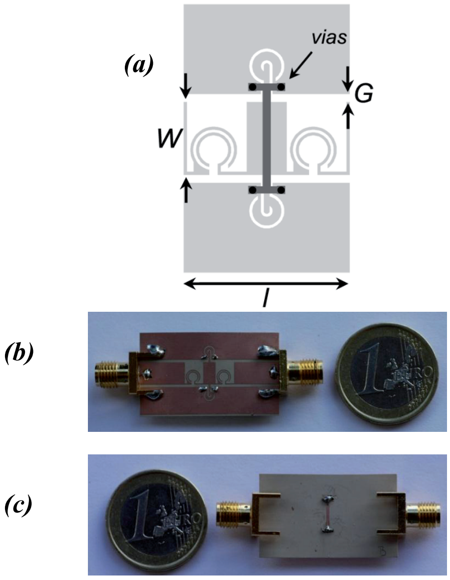

Fig. 5. Layout (a) and top (b) - bottom (c) photograph of the CPW wideband band-pass filter based on a combination of series connected OSRRs in the external stages and a pair of shunt connected OCSRRs in the central stage. Dimensions are: $l = 9$ mm, $W = 5$ mm and $G = 0.55$ mm. For the OCSRR: $r_{ext} = 1.2$ mm, $c = 0.2$ mm and $d = 0.6$ mm. For the OSRR: $r_{ext} = 1.6$ mm and $c = d = 0.2$ mm.

Fig. 6(a) shows the electromagnetic and circuit simulation of the filter without losses, considering for comparison purposes both the simple and wideband OCSRR model (i.e., considering the case with and without the additional parameter L_{sh} in reference of Fig. 4a). As can be appreciated, since the fractional bandwidth of the filter is moderate, the simple OCSRR model can still predict the band, although it begins to fail at higher frequencies. Fig. 6(b) also shows the wideband frequency response of the electromagnetic simulation considering dielectric, conductor and radiation losses, the circuit and ideal Chebyshev models, as well as the measurement of the fabricated device. The group delay and insertion loss of the electromagnetic simulation and measurement are also depicted in Fig. 6(c). There is good agreement between all the curves in the region of interest, with the first spurious band at roughly 2.3 times the central filter frequency. Measured filter characteristics are good with insertion losses lower than 1 dB between 2.3 GHz and 3.5 GHz, and measured return losses better than 18 dB between 2.36 GHz and 3.41 GHz.

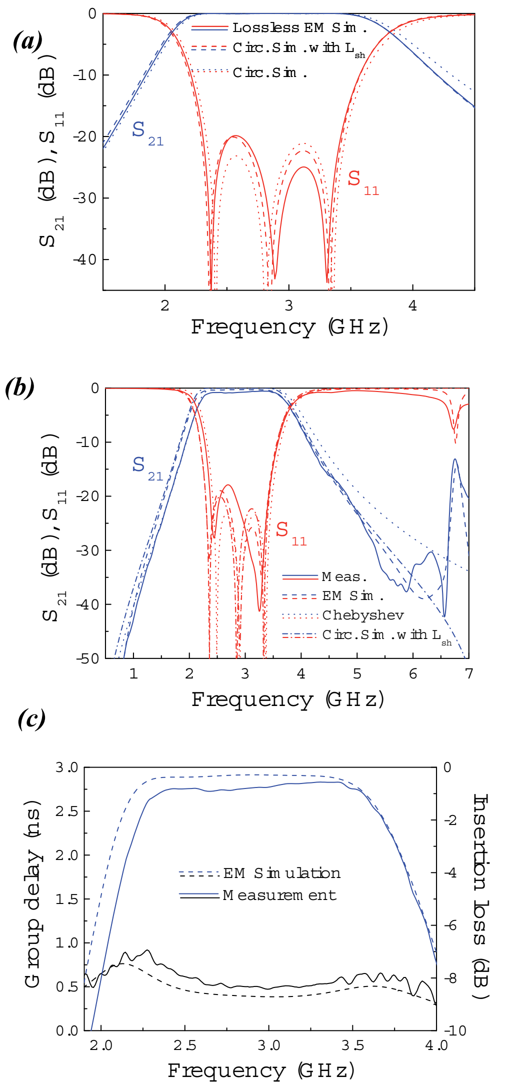

Fig. 6. Frequency response simulation without losses (a); Wideband frequency response simulation with losses and measurement (b); Group delay and detail of the insertion loss of the circuit of Fig. 5. The Chebyshev element values obtained from the band-pass prototype transformations, in reference to Fig. 1 (where $L = C = 0$), are: C_s= 0.54 pF, L'_p= 0.93 nH, C'_p= 3.3 pF and L'_s= 5.76 nH. The values of the circuit simulation considering parasitics, inferred from parameter extraction method, are: C = 0.19 pF, L = 0.4 nH, C_s = 0.58 pF, L'_s = 5.55 nH, C'_p = 3 pF and L'_p = 0.94 nH. The modified values of the OCSRR considering the wideband model with the additional parasitic element L_{sh} are (in reference to Fig. 4a): L = 0.345 nH, C'_p = 2.98 pF, L'_p = 0.94 nH and L_{sh} = 0.19 nH.

Furthermore, the circuit simulation considering the parasitic element L_{sh} predicts both the band-pass and the stop-band rejection, where due to this additional shunt inductance behavior, these types of filters will have the advantage of a more selective upper transition band compared to the Chebyshev responses, as well as an additional transmission zero above the band (present at higher frequencies than those depicted for the filter shown).

Nonetheless, if either the order or the parasitic element values dramatically increase, the manual tuning of the whole structure at the circuit level can be a complex and time consuming task. In these latter circumstances, an automatic optimization routine that forces the frequency positions at the N matching points of the Chebyshev response (i.e., where the input impedance is 50 Ω) can be implemented in a commercial simulator such as *Agilent ADS*, with N being the filter order. Hence, by predefining the frequency matching positions (which are given by the Chebyshev prototype response), the optimum circuit elements considering a set of fixed parasitics values can be obtained for any filter order or any fixed parasitic value through an automatic iterative process. However, the element values as well as their possible swept ranges should be chosen to be close to the optimal final solution in order to achieve converge with the response that satisfies the required specifications (i.e., ripple and bandwidth). To this purpose, the circuit elements inferred by the parameter extraction method can be considered as starting point. These circuit elements should be the same or close to the canonical circuit model elements, given that the magnitudes of the parasitics do not dramatically alter the final optimal values as compared to the initial canonical circuit elements. Hence, the requirements can be met.

As an example, this routine is applied to the already designed filter, where the final circuit elements inferred by the parameter extraction method are considered as a starting point and optimized to fulfill the initial filter requirements considering constant parasitics (since these are the only non-controllable parameters). Fig. 7 shows the frequency response comparison between the circuit model and the Chebyshev response. As can be observed, if the simple OCSRR model is considered, a nearly perfect fit between both curves is obtained with this method, with a slight deviation only on the stop-band rejection at high frequencies. On the other hand, if the same method is considered with the wideband model of the OCSRR (i.e., considering the additional inductance L_{sh}) it can be seen how the same goals are achieved, but with a slight discrepancy in return loss, as well as a higher upper selectivity due to this factor.

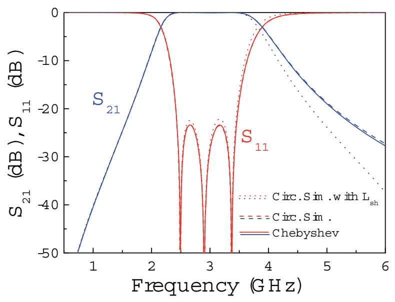

Fig. 7. Frequency response comparison between the ideal Chebyshev and circuit simulation obtained by automatic matching point optimization considering both the simple and wideband model of the OCSRR. The circuit values are: For the case of considering the simple OCSRR model (in reference to Fig. 1a): C = 0.19 pF, L = 0.4 nH, C_s = 0.55 pF, L'_s= 5.57 nH, C'_p= 3.17 pF and L'_p= 0.86 nH. For the case of considering the wideband OCSRR model (in reference to Fig. 4): C = 0.19 pF, L = 0.4 nH, L_{sh} = 0.19 nH, C_s= 0.52 pF, L'_s= 5.76 nH, C'_p= 3.24 pF and L'_p= 0.8 nH.

5. Further Illustrative Examples

Once the design procedure has been established, the limitation of this approach is studied by designing different types of bandwidths and filter orders. In order to correctly compare the above presented filter with the forthcoming different ripple filters, the -3 dB fractional bandwidth parameter FBW_{-3dB} can be considered, related to the fractional bandwidth of a Chebyshev filter FBW as [13]

$$\frac{FBW_{-3dB}}{FBW} = \cosh\left[\frac{1}{N}\cdot \operatorname{acosh}\left(\frac{1}{\sqrt{10^{0.1\cdot ripple}-1}}\right)\right] \tag{8}$$

where N is the order of the filter and the ripple is given in decibels. Therefore, if a Chebyshev response with 3 dB ripple is considered, the hyperbolic arccosine is zero and the ratio of fractional bandwidth reduces to unity as expected, since both fractional bandwidths are the same in this case. In a similar manner, the above designed filter with 35% FBW presents a FBW_{-3dB} = 60%. Additionally, two third-order filters with f_0 = 2 GHz, ripple of 0.15 dB and fractional bandwidth of 70% (FBW_{-3dB} = 93%) and 90% (FBW_{-3dB} = 119%), respectively, have been designed. The layouts and photographs of each filter are shown in Fig. 8. In Fig. 9(a)-(b) the lossless frequency response comparison of these filters is shown, including the electromagnetic simulation and the circuit simulation, considering the simple and wideband OCSRR model (i.e., with and without considering L_{sh}). In Fig. 9(c)-(d) the wideband frequency response of these filters including measurement is depicted.

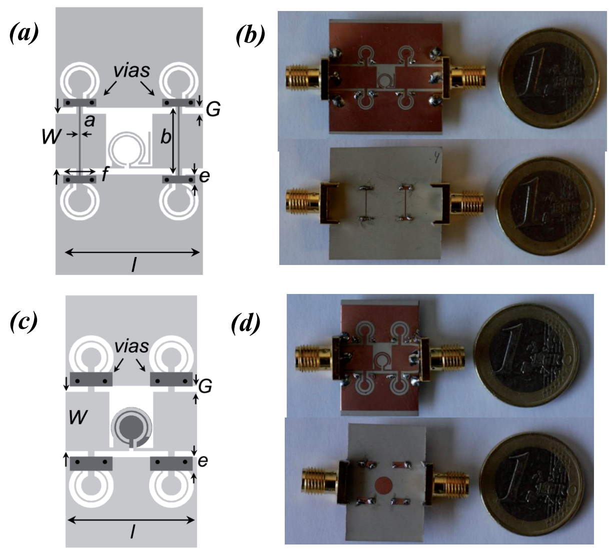

Fig. 8. Topology (a), (c) and photograph (b), (d) of the designed third-order filter with 70% and 90% fractional bandwidth, respectively. The considered substrate is the *Rogers RO3010* with thickness h = 0.254 mm and measured dielectric constant ε_r = 11.2. Dimensions are: (a)-(b): l = 13.38 mm, W = 5 mm, G = 0.547 mm, a = 0.16 mm, b = 6.27 mm, e = 0.73 mm, f = 3 mm. For the OCSRR: r_{ext}= 1.8 mm, c = 0.3 mm, d = 0.16 mm. For the OSRR: r_{ext}= 1.7mm, c = d = 0.16mm. (c) - (d): l = 12.32 mm, W = 5.6 mm, G = 0.574 mm, e = 1.34 mm. For the OCSRR: r_{ext}=2.1 mm, c= 0.5 mm, d =0.16 mm. For the OSRR: r_{ext}= 1.9 mm, c = 0.3 mm, d = 0.16 mm.

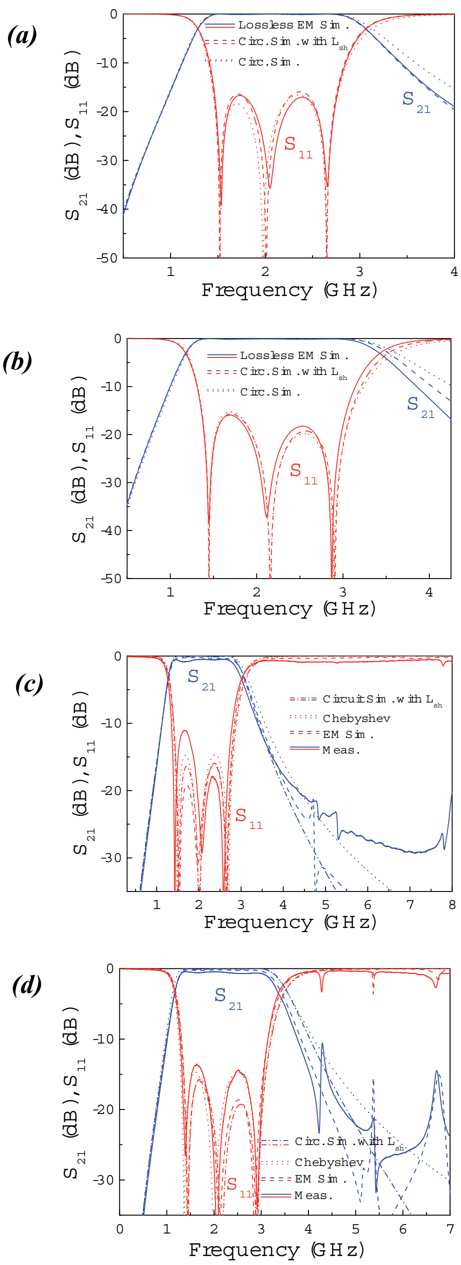

Fig. 9. Frequency response without losses (a), (b) and wideband frequency response (c), (d) of the designed third-order filter with 70% and 90% fractional bandwidth, respectively. The values of the circuit simulation considering parasitics, inferred from parameter extraction method, are (in reference to Fig. 1): (a), (c): C = 0.188 pF, L = 0.62 nH, C_s= 0.85 pF, L'_s= 6.3 nH, C'_p= 2.43 pF, L'_p= 2.7 nH. (b), (d): L = 0.384 nH, C'_p= 1.79 pF, L'_p = 3.2 nH, C_s = 1.08 pF, L'_s = 4.89 nH, C = 0.182 pF. The modified values of the OCSRR considering the wideband model with the additional parasitic element L_{sh} are (in reference to Fig. 4): (a), (c): L = 0.62 nH, C'_p = 2.54 pF, L'_p = 2.56 nH, L_{sh}= 0.15 nH. (b), (d): L = 0.384 nH, C'_p = 1.779 pF, L'_p= 3.216 nH and L_{sh} = 0.2 nH.

As can be seen, the higher the bandwidth, the worse the model prediction of the upper transition band. Nonetheless, the wideband model of the OCSRR has been proven to be useful for filters with fractional bandwidths as high as 90%. For higher bandwidth requirements, the model will not accurately predict the upper transition band due to the limited range of operation of the lumped element equivalent circuit model. However, since the limitation to design wider band filters would come only from the model rather than from the layout, it would still be possible to consider this approach for wider band filters, where enhanced nominal bandwidths in the design could be considered to compensate the model inaccuracies. Good agreement between the measured frequency responses and the simulations is obtained. Wide stop-bands are achieved in both cases (the 70% fractional bandwidth filter is free of spurious bands in the depicted range, i.e., four times the central filter frequency). Filter size is as small as $0.13\lambda_g \times 0.15\lambda_g$ and $0.13\lambda_g \times 0.17\lambda_g$ for the 70% and 90% fractional bandwidth filter, respectively, where λ_g is the guided wavelength at the central filter frequency.

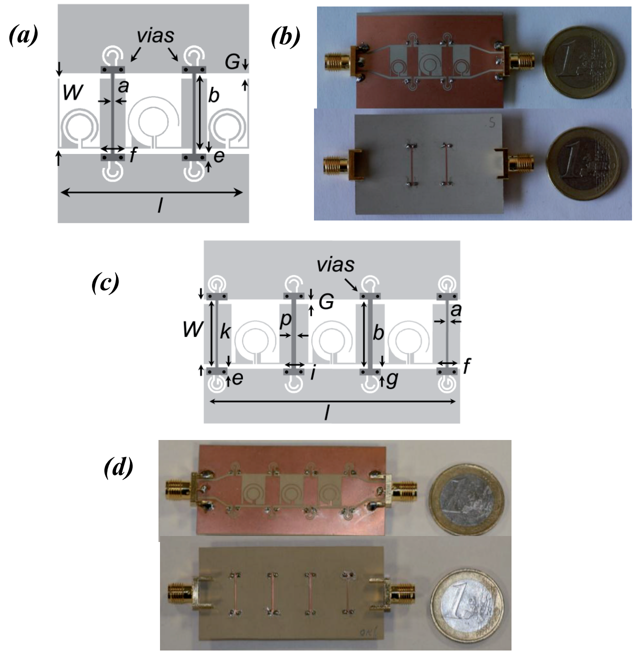

Fig. 10. Topology (a), (c) and photograph (b), (d) of the designed fifth- and seventh-order filter, respectively. The considered substrate is the *Rogers RO3010* with thickness h = 0.254 mm and measured dielectric constant ε_r = 11.2. Dimensions are: (a), (b): l = 25 mm, W = 9.23 mm, G = 0.71 mm, a = 0.4 mm, b = 10.64 mm, e = 0.96 mm and f = 3.2 mm. For the external OSRRs: r_{ext} = 2.5 mm, c = 0.3 mm and d = 0.35 mm. For the central OSRR: r_{ext} = 3.4 mm, c = 0.16 mm and d = 1.24 mm. For the OCSRRs: r_{ext} = 1.4 mm and c = d = 0.3 mm. (c), (d): l = 39.16 mm, W = 9.23 mm, G = 0.712 mm, a = 0.35 mm, b = 10.63 mm, e = 1.19 mm, f = I = 3.2 mm, g = 1 mm, k = 10.3 mm and p = 0.71 mm. For the OCSRRs of stages 1 and 7, r_{ext} = 1.4 mm, c = 0.3 mm and d = 0.2 mm; For the OCSRRs of stages 3 and 5, r_{ext} = 1.4 mm, c = 0.3 mm and d = 0.3mm; For the OSRRs of stages 2, 4 and 6, r_{ext} = 3.2 mm, c = 0.16 mm and d = 1.02 mm.

Higher order structures have also been studied [12], [14]. An order-5 Chebyshev filter with f_0 = 2 GHz, ripple of 0.05 dB and fractional bandwidth of 50% (FBW_{-3dB} = 59%) and an order-7 filter with f_0= 1.87 GHz, ripple of 0.25 dB and fractional bandwidth of 53% (FBW_{-3dB} =

55%), have been designed. The layouts and photographs of these filters are shown in Fig. 10 and the frequency response in Fig. 11.

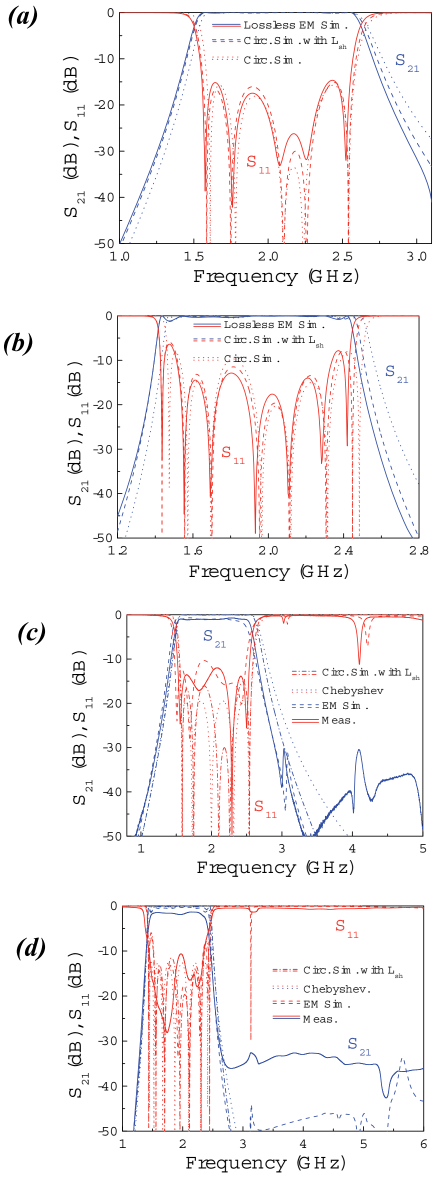

Fig. 11. Frequency response without losses (a), (b) and wide-band frequency response (c), (d) of the designed fifth- and seventh-order filter, respectively. The element values for the circuit simulation without considering L_{sh} are (in reference to Fig. 1): (a), (c): For the external OSRRs: C = 0.207 pF, C_s = 0.763 pF, L'_s = 8.501 nH. For the central OSRR: C = 0.274 pF, C_s = 0.436 pF, L'_s= 13.118 nH. For the OCSRRs: L = 0.474 nH, C'_p = 4.5 pF, L'_p= 1.224 nH. (b), (d): For the OCSRRs of stages 1 and 7, L'_p= 1.56 nH, C'_p= 4.34 pF, L = 0.47 nH; For the OCSRRs of stages 3 and 5, L'_p= 0.979 nH, C'_p = 6.46 pF, L = 0.501 nH; For the OSRRs of stages 2, 4 and 6, L'_s = 11 nH, C_s = 0.588 pF, C = 0.26 pF. The modified values of the OCSRR considering the wideband model with the additional parasitic element L_{sh} are (in reference to Fig. 4): (a), (c) L = 0.385 nH, C'_p = 4.4 pF, L'_p = 1.259 nH, L_{sh} = 0.35 nH. (b), (d): For the OCSRRs of stages 1 and 7, L'_p = 1.56 nH, C'_p = 4.35 pF, L = 0.48 nH, L_{sh}= 0.31 nH; For the OCSRRs of stages 3 and 5, L'_p= 1.009 nH, C'_p = 6.28 pF, L = 0.501 nH, L_{sh} = 0.33 nH.

From this analysis, it can be deduced that the parameter L_{sh} has to be also considered for high order filters although the bandwidth of the filter is relatively small compared to the cases analyzed before. This is because the small error of the simple OCSRR model is multiplied for each OCSRR stage, resulting in higher inaccuracies both below and above the band as the order increases (whereas for low order filters the simple OCSRR only results in inaccuracies above the band).

This phenomenon can be clearly appreciated in Fig. 11(b), where the seventh-order filter presents a very good agreement between the circuit and electromagnetic response around the band-pass but tends to fail at the edges if the parameter L_{sh} is not considered. On the other hand, it is demonstrated that the design of high order filters is also possible with this approach if the wideband model of the OCSRR is considered, obtaining similar results in measurement (although higher losses are observed for the seventh-order filter due to the non-consideration of conductor losses and fabrication tolerances). In addition, a high selectivity is obtained, with a rejection level better than - 30 dB for at least $2.5f_0$ and $3f_0$, with filter dimensions as small as $0.24\lambda_g \times 0.17\lambda_g$ and $0.37\lambda_g \times 0.17\lambda_g$ for the fifth- and seventh-order filter, respectively.

6. Conclusion

High-order CPW broadband bandpass filters have been implemented by combining OSRRs and OCSRRs. The main relevant aspects of this paper have been the introduction of an inductance L_{sh} in the OCSRR circuit model to better describe the wideband response of the particle, as well as the proposal of an optimization routine for filter design. With these aspects, it has been found that the models provide a good description of the proposed filters, and the design of filters subjected to specifications can be achieved.

Acknowledgement

This work has been supported by Spain-MICIIN (project contract TEC2010-17512 METATRANSFER). Thanks are also given to the Catalan Government (CIDEM/COPCA) for funding CIMITEC and for giving us support through the project SGR2009-421. This work has been also supported through the CONSOLIDER-INGENIO 2010 program (Spain-MICIIN) under project number CSD2008-00066. Ferran Martin is in debt with the ICREA Foundation for giving him an ICREA Academia award.

References

[1] PENDRY, J.B., HOLDEN, A.J., ROBBINS, D.J., STEWART, W.J. Magnetism from conductors and enhanced nonlinear

phenomena. *IEEE Transactions Microwave Theory Tech.*, 1999, vol. 47, p. 2075-2084.

[2] FALCONE, F., LOPETEGI, T., BAENA, J.D., MARQUÉS, R., MARTÍN, F., SOROLLA, M. Effective negative-ε stop-band microstrip lines based on complementary split ring resonators. *IEEE Microwave and Wireless Components Letters*, June 2004, vol. 14, p. 280-282.

[3] BILOTTI, F., TOSCANO, A., VEGNI, L. Design of spiral and multiple split-ring resonators for the realization of miniaturized metamaterial samples. *IEEE Transactions on Antennas and Propagation*, August 2007, vol. 55, p. 2258-2267.

[4] BILOTTI, F., TOSCANO, A., VEGNI, L., ALICI, K.B., AYDIN, K., OZBAY, E. Equivalent circuit models for the design of metamaterials based on artificial magnetic inclusions. *IEEE Transactions on Microwave Theory and Techniques*, December 2007, vol. 55, p. 2865-2873.

[5] GIL, I., BONACHE, J., GIL, M., GARCÍA-GARCÍA, J., MARTÍN, F. Left handed and rigth handed transmission properties of microstrip lines loaded with complementary split rings resonators. *Microwave and Optical Technology Letters*, December 2006, vol. 48, p. 2508-2511.

[6] GIL, M., BONACHE, J., SELGA, J., GARCÍA-GARCÍA, J., MARTÍN, F. Broadband resonant type metamaterial transmission lines. *IEEE Microwave and Wireless Components Letters*, vol. 17, February 2007, p. 97-99.

[7] GIL, M., BONACHE, J., GARCÍA-GARCÍA, J., MARTEL, J., MARTÍN, F. Composite right/left handed (CRLH) metamaterial transmission lines based on complementary split rings resonators (CSRRs) and their applications to very wide band and compact filter design. *IEEE Transactions on Microwave Theory and Techniques*, June 2007, vol. 55, p. 1296-1304.

[8] MARTEL, J., MARQUÉS, R., FALCONE, F., BAENA, J.D., MEDINA, F., MARTÍN, F., SOROLLA, M. A new LC series element for compact bandpass filter design. *IEEE Microwave Wireless Components Letters*, May 2004, vol. 14, p. 210-212.

[9] VELEZ, A., AZNAR, F., BONACHE, J., VELÁZQUEZ-AHUMADA, M.C., MARTEL, J., MARTÍN, F. Open complementary split ring resonators (OCSRRs) and their application to wideband CPW bandpass filters. *IEEE Microwave and Wireless Components Letters*, April 2009, vol. 19, p. 197-199.

[10] DURÁN-SINDREU, M., VÉLEZ, A., AZNAR, F., SISÓ, G., BONACHE, J., MARTÍN, F. Application of open split ring resonators and open complementary split ring resonators to the synthesis of artificial transmission lines and microwave passive components. *IEEE Trans. Microwave Theory and Techniques*, Dec. 2009, vol. 57, p. 3395-3403.

[11] DURÁN-SINDREU, M., VÉLEZ, P., BONACHE, J., MARTÍN, F. Broadband microwave filters based on metamaterial concepts. In *20th International Conference on Applied Electromagnetics and Communications*. Dubrovnik (Croatia), 20 – 23 September 2010.

[12] DURÁN-SINDREU, M., VÉLEZ, P., BONACHE, J., MARTÍN, F. High-order coplanar waveguide (CPW) filters implemented by means of open split ring resonators (OSRRs) and open complementary split ring resonators (OCSRRs). *Metamaterials*, accepted (DOI: 10.1016/ j.metmat.2011.03.002).

[13] DISHAL, M. Design of dissipative band-pass filters producing desired exact amplitude-frequency characteristics. *Proceedings of the I.R.E.*, September 1949, vol. 37, p. 1050-1069.

[14] DURÁN-SINDREU, M., VÉLEZ, A., SISÓ, G., VÉLEZ, P., SELGA, J., BONACHE, J., MARTÍN, F. Recent advances in metamaterial transmission lines based on split rings. *Proceedings of the IEEE*, accepted (DOI: 10.1109/JPROC.2011.2114870).

About Authors …

Miguel DURÁN-SINDREU was born in 1985 in Barcelona (Spain). He received the Telecommunications Engineering Diploma, specializing in Electronics, the Telecommunications Engineering degree and the Ph.D. degree in 2007, 2008 and 2011, respectively, from the Universitat Autònoma de Barcelona. His research interests are microwave filters, metamaterials and multi-band components.

Paris VÉLEZ was born in Barcelona (Spain) in 1982. He received the Telecommunication Technical Engineering Diploma (specialty in Electronics) from the Universitat Autònoma de Barcelona (UAB) in 2007 and the Electronics Engineering degree in 2010. He is currently working towards the Ph.D. degree in subjects related to the miniaturization of metamaterial based RF and microwave passive circuits.

Jordi BONACHE was born in Cardona (Barcelona), Spain, in 1976. He received the Physics and Electronics Engineering degrees and Ph.D. degree in Electronics Engineering from the Universitat Autònoma de Barcelona, Bellaterra (Barcelona), Spain, in 1999, 2001, and 2007, respectively. In 2000, he joined the High Energy Physics Institute of Barcelona (IFAE), where he was involved in the design and implementation of the control and monitoring system of the MAGIC telescope. In 2001, he joined the Department d'Enginyeria Electrònica, Universitat Autònoma de Barcelona, where he is currently an Assistant Professor. His research interests include active and passive microwave devices and metamaterials.

Ferran MARTÍN was born in Barakaldo (Vizcaya), Spain in 1965. He received the B.S. Degree in Physics from the Universitat Autònoma de Barcelona (UAB) in 1988 and the PhD degree in 1992. From 1994 up to 2006 he has been an Associate Professor in Electronics at the Departament d'Enginyeria Electrònica (Universitat Autònoma de Barcelona), and from 2007 he is a Full Professor of Electronics. In recent years, he has been involved in different research activities including modeling and simulation of electron devices for high frequency applications, millimeter wave and THz generation systems, and the application of electromagnetic bandgaps to microwave and millimeter wave circuits. He is now very active in the field of metamaterials and their application to the miniaturization and optimization of microwave circuits and antennas. He is the head of the Microwave and Millimeter Wave Engineering Group (GEMMA Group) at UAB, and director of CIMITEC, a research Center on Metamaterials supported by TECNIO (Generalitat de Catalunya). He has organized several international events related to metamaterials, including Workshops at the IEEE International Microwave Symposium (2005 and 2007) and European Microwave Conference (2009). He has acted as Guest Editor for three Special Issues on Metamaterials in three International Journals. He has authored and co-authored over 300 technical conference, letter and journal papers and he is coauthor of the monograph on Metamaterials entitled Metamaterials with Negative Parameters: Theory, Design and Microwave Applications (John Wiley & Sons Inc.). Ferran Martín has filed several patents on metamaterials and has headed several Development Contracts. Among his distinctions, Ferran Martín has received the 2006 Duran Farell Prize for Technological Research, he holds the Parc de Recerca UAB – Santander Technology Transfer Chair, and he has been the recipient of an ICREA ACADEMIA Award.

RADIOENGINEERING REVIEWERS I

December 2011, Volume 20, Number 4

- ABUELMA’ATTI, M. T., King Fahd University of Petroleum & Minerals, Saudi Arabia
- ARCE-DIEGO, J. L., University of Cantabria, Santander, Spain
- ASHBURNER, J., UCL, London, UK
- BALLING, P., Antenna Systems Consulting ApS, Denmark
- BAROŇÁK, I., Slovak University of Technology, Bratislava, Slovakia
- BEČVÁŘ, Z., Czech Technical University in Prague, Czechia
- BILÍK, V., Slovak University of Technology, Bratislava, Slovakia
- BILOTTI, F., Roma Tre University, Italy
- BIOLEK, D., University of Defense, Brno, Czechia
- BOBULA, M., RACOM company, Czechia
- BONEFAČIĆ, D., University of Zagreb, Croatia
- CHAUDRY, A., Panjab University, India
- COSTANZO, S., University of Calabria, Italy
- ČAPEK, M., Czech Technical University in Prague, Czechia
- ČERNOCKÝ, J., Brno University of Technology, Czechia
- ČERNÝ, P., Czech Technical University in Prague, Czechia
- ČÍKA, P., Brno University of Technology, Czechia
- DE SOUZA, R., National Institute of Telecommunications, Brazil
- DEL-RIO, C., University of Navarra, Spain
- DJIGAN, V., R&D Center of Microelectronics, Russia
- DOBEŠ, J., Czech Technical University in Prague, Czechia
- DROTÁR, P., Honeywell International, Czechia
- DŘÍNOVSKÝ, J., Brno University of Technology, Czechia
- ELHADJ, Z., University of Tébéssa, Algeria
- FANJUL-VÉLEZ, F., University of Cantabria, Spain
- FEDRA, Z., Brno University of Technology, Czechia
- FONTAN, P. F., University of Vigo, Spain
- GAI, Y., University of Southern California, USA
- GAZDA, J., Technical University of Košice, Slovakia
- GEORGIADIS, A., Centre Tecnologic de Telecomunicacions de Catalunya, Barcelona, Spain
- GOŇA, S., Tomas Bata University in Zlin, Czechia
- GRGIĆ, S., University of Zagreb, Croatia
- HANÁČEK, P., Brno Univ. of Technology, Czechia
- HAZDRA, P., Czech Technical University in Prague, Czechia
- HÁJEK, K., University of Defense, Brno, Czechia
- HÁZE, J., Brno University of Technology, Czechia
- HEKRDLA, M., Czech Technical University in Prague, Czechia
- HERENCSÁR, N., Brno University of Technology, Czechia
- HORNG, J.-W., Chung Yuan Christian University, Taiwan
- HORSKÝ, P., AMIS Czech, Ltd., Brno, Czechia
- HRABAR, S., University of Zagreb, Croatia
- HUDEC, P., Czech Technical University in Prague, Czechia

- JABRI, F., University of Technology, Iraq
- JAIKLA, W., Suan Sunandha Rajabhat University, Thailand
- JAKOVENKO, J., Czech Technical University in Prague, Czechia
- JAN, J., Brno University of Technology, Czechia
- JIŘÍK, R., Academy of Sciences of the Czech Republic, Czechia
- KESKIN, A. U., Yeditepe University, Istanbul, Turkey
- KHATEB, F., Brno Univ. of Technology, Czechia
- KOCUR, D., Technical Univ. of Košice, Slovakia
- KOLKA, Z., Brno Univ. of Technology, Czechia
- KOLÁŘ, R., Brno Univ. of Technology, Czechia
- KOS, T., University of Zagreb, Croatia
- KOVÁŘ, P., Czech Technical University in Prague, Czechia
- KUBÍČEK, M., Brno Univ. of Technology, Czechia
- KUČERA, P., Pforzheim University, Germany
- KULLA, P., Slovak University of Technology, Bratislava, Slovakia
- KVIČERA, M., Czech Technical University in Prague, Czechia
- LAHIRI, A., Netaji Subhas Institute of Technology, New Delhi, India
- LAKKUNDI, V., FORTH-ICS, Heraklion, Greece
- LÁČÍK, J., Brno University of Technology, Czechia
- LEE, S.-K., Yuan Ze University, Taiwan
- LEONE, M., Otto-von-Guericke-Universitat, Magdeburg, Germany
- LEVICKÝ, D., Technical Univ. of Košice, Slovakia
- LI, L., UESTC, China
- LOPEZ-VALCARCE, R., University of Vigo, Spain
- LUKEŠ, Z., Brno University of Technology, Czechia
- LUXEY, C., University of Nice-Sophia Antipolis, France
- MAHESHWARI, S., Aligarh Muslim University, Utar Pradesh, India
- MARŠÁLEK, R., Brno University of Technology, Czechia
- MARTIN, F., Universitat Autonoma de Barcelona, Spain
- MARTINEZ-VAZQUEZ, M., IMST GmbH, Kamp-Lintfort, Germany
- MASLENNIKOV, R., University of Nizhny Novgorod, Russia
- MINAEI, S., Dogus University, Turkey
- MENZE, B., ETH Zurich, Switzerland
- MERISAARI, H., Turku University, Finland
- MORÁVEK, O., Czech Technical University in Prague, Czechia
- MOURAD, F., University of Sfax, Tunisia
- NAGY, J., Brno University of Technology, Czechia
- NOVOTNÝ, V., Brno Univ. of Technology, Czechia
- OPPL, L., Czech Technical University in Prague, Czechia
- OZEN, A., Karadeniz Technical University, Turkey
- OZOGUZ, S., Istanbul Technical University, Turkey
- PENNA, F., Politecnico di Torino, Italy
- POLÁK, L., Brno University of Technology, Czechia
- POLÍVKA, M., Czech Technical University in Prague, Czechia
- POVALAČ, A., Brno Univ. of Technology, Czechia
- PROKEŠ, A., Brno Univ. of Technology, Czechia
- PROKOP, R., Brno Univ. of Technology, Czechia
- PUSKELY, J., Brno Univ. of Technology, Czechia
- RABOCH, J., Czech Technical University in Prague, Czechia
- RAIDA, Z., Brno University of Technology, Czechia
- RÓKA, R., Slovak University of Technology, Bratislava, Slovakia
- ŘÍHA, K., Brno University of Technology, Czechia
- SCHEJBAL, V., University of Pardubice, Jan Perner Transport Faculty, Czechia
- SCHWARZ, D., Masaryk University, Brno, Czechia
- SEGOVIA-VARGAS, D., Carlos III University of Madrid, Spain
- SENANI, R., Netaji Subhas Institute of Technology, New Delhi, India
- SIZOV, V., University of Birmingham, UK
- SIRIPRUCHYANUN, M., King Mongkut's University of Technology North Bangkok, Thailand
- SKRIVERVIK, A., EPFL, Switzerland
- SLANINA, M., Brno Univ. of Technology, Czechia
- SMÉKAL, Z., Brno University of Technology, Czechia
- SOLIMAN, A., Cairo University, Egypt